A continuum-microscopic method based on IRBFs and control volume scheme for viscoelastic fluid flows

C.-D. Tran, N. Mai-Duy, K. Le-Cao, and T. Tran-Cong

Computational Engineering and Science Research Centre
Faculty of Engineering and Surveying
The University of Southern Queensland, Toowoomba, QLD 4350, Australia.

Abstract: A numerical computation of continuum-microscopic model for viscoelastic flows based on the Integrated Radial Basis Function (IRBF) Control Volume and the Stochastic Simulation Techniques (SST) is reported in this paper. The macroscopic flow equations are closed by a stochastic equation for the extra stress at the microscopic level. The former are discretised by a 1D-IRBF-CV method while the latter is integrated with Euler explicit or Predictor-Corrector schemes. Modelling is very efficient as it is based on Cartesian grid, while the integrated RBF approach enhances both the stability of the procedure and the accuracy of the solution. The proposed method is demonstrated with the solution of the start-up Couette flow of the Hookean and FENE dumbbell model fluids.

Keywords: Stochastic simulation techniques, Brownian configuration fields, Integrated radial basis functions, Control volume, Viscoelastic fluid flow, Continuum-microscopic method.

1 Introduction

For the last several decades, multi-scale problems have attracted significant attention across several fields, including mathematics, engineering, chemistry, materials science, biology and fluid dynamics [Weinan and Engquist (2003)]. A number of analytic and numerical methods for multi-scale problems have been developed [Kevorkian and Cole (1996); Maslov and Fedoriuk (1981); Engquist, Lötstedt, and Runborg (2000); Hou (2005); Chu, Efendiev, Ginting, and Hou (2008); Hajibeygi, Gonfigli, Hesse, and Jenny (2008)]. A simple brute force discretisation, that can capture small scale features, will result in prohibitively expensive numerical procedures. Thus it is necessary to devise multi-scale strategies where small scale features can be captured effectively and efficiently within an overall practically realisable macroscopic procedure. In such multi-scale strategies, different physical laws are often required to describe the system at different scales. For example, at the macro-scale, complex fluids are accurately described by the velocity, pressure, and temperature fields, which satisfy the physical conservation equations while on

the micro-scale, it is necessary to use kinetic theory to get a more detailed description in terms of the probability distribution function of particles [Bird, Armstrong, and Hassager (1987)]. Thus, rheological properties at the macroscopic level can be solved by a multi-scale strategy consisting in searching for the information on the microstructures of the fluids. The information is then used to solve the macroscopic governing equations. This continuum-microscopic (also known as macro-micro) multi-scale approach does not require closed form constitutive equations [Ottinger (1996)]. The approach is an attempt to emulate the situation in real liquids, where the full information about the stress is contained in the configuration of molecules which results from the micro-scale deformation history. The main idea of these techniques is that the polymer contribution to the stress is directly calculated from a large ensemble of microscopic configurations without having to derive a closed form constitutive equation, which is a powerful feature for the modelling of materials [Engquist, Lötstedt, and Runborg (2000)]. On the computational side, several numerical techniques have been developed for the continuum-microscopic multi-scale approach [Laso and Ottinger (1993); Hulsen, van Heel, and van den Brule (1997); Somasi and Khomami (2001); Jourdain, Lelièvre, and Bris (2002); Tran-Canh and Tran-Cong (2002); Keunings (2004); Tran, Phillips, and Tran-Cong (2009)].

Recently, a numerical scheme based on the combination of 1D-IRBFNs collocation and SST for the analysis of visco-elastic fluid flows showed a significant improvement of the approximation accuracy owing to a reduction in the approximation noise caused by differentiation [Tran, An-Vo, Mai-Duy, and Tran-Cong (2011)]. Owing to the advantages of a Control Volume technique, including the conservative nature and the ability of handling domains with complex geometry, the present work will present a 1D-IRBF based Control Volume method [Mai-Duy and Tran-Cong (2010)] incorporating the Brownian Configuration Fields (BCF) technique for a continuum-microstructure model of viscoelastic flows. The present approach achieves high-order convergence and accuracy.

The paper is organized as follows. Section 2 presents an overview of the governing equations of non-Newtonian fluid flows for the macroscopic approach. In section 3, the simulation method of BCF is described for the computation of the polymer contributed stress. A continuum-microscopic multi-scale system of equations governing the flow of dumbbell model fluids are introduced in section 4. The numerical solution of the coupled continuum-microscopic equations is detailed in section 5 where the BCF and the 1D-IRBFN control volume methods are presented. An algorithm of the present procedure is presented to describe the discretizations of the continuum and microstructure components as well as their interaction. Numerical examples are then discussed in section 6 with a conclusion in section 7.

2 Governing equations for non-Newtonian fluid flows

Consider the isothermal flow of an incompressible complex fluid, the system of momentum and mass conservation equations is given by

$$\rho \frac{D}{Dt}(\mathbf{u}) = -\nabla p + \nabla \cdot \tau, \tag{1}$$

$$\nabla \cdot \mathbf{u} = 0, \tag{2}$$

where ρ is the density, p the pressure arisen due to the incompressibility constraint; $\mathbf{u}$ the velocity field; and τ the extra stress. The extra stress is then further decomposed as

$$\tau = \tau_s + \tau_p, \tag{3}$$

where $\tau_s = 2\eta_s \mathbf{D}$ is the Newtonian solvent contribution to the stress; η_s the solvent viscosity; $\mathbf{D} = 0.5\left(\nabla \mathbf{u} + (\nabla \mathbf{u})^T\right)$ the rate of strain tensor; τ_p the polymer-contributed stress; and $\frac{D}{Dt}(\cdot) = \frac{\partial}{\partial t}(\cdot) + (\mathbf{u} \cdot \nabla)(\cdot)$ the substantial derivative.
For a given model material, the polymer contribution to the stress (τ_p) is governed by specific equations that may lead to a constitutive equation of the form

$$\frac{D(\tau_p)}{Dt} = f(\tau_p, \nabla \mathbf{u}). \tag{4}$$

In the macroscopic methods of analysis, the conservation equations (1) & (2) are closed by a constitutive equation such as (4). In contrast, if a closed form constitutive equation cannot be obtained, the conservation equations (1) and (2) can be closed by equations governing the evolution of the microscopic structures of the fluid in continuum-microscopic multi-scale approaches, of which one is described in the next section.

3 A microscopic stochastic simulation method

We consider dumbbell models at the microscopic level. Microscopic models can be simulated using different approaches. In this work, the BCF scheme is used. In this procedure, an equation at the microscopic level describes the evolution of the microstructures, leading to the computation of the non-Newtonian contribution τ_p to the stress. Each dumbbell consists of two Brownian beads which are connected together by a spring. The configuration of a dumbbell is completely described by the length and orientation of the end-to-end vector $\mathbf{R}$ connecting the two beads (see Ottinger (1996) for more details). The evolution of $\mathbf{R}$ is modeled using a stochastic

differential equation as follows.

$$d\mathbf{R}(t,\mathbf{x}) = \left[-\mathbf{u}(t,\mathbf{x})\cdot\nabla\mathbf{R}(t,\mathbf{x}) + \nabla\mathbf{u}(t,\mathbf{x})\cdot\mathbf{R}(t,\mathbf{x}) - \frac{2}{\zeta}\mathbf{F}(\mathbf{R}(t,\mathbf{x}))\right]dt + \sqrt{\frac{k_B T}{\zeta}}d\mathbf{Z}(t), \tag{5}$$

where $\mathbf{u}$ is the velocity field; ζ the friction coefficient between the dumbbell and the solvent; k_B the Boltzmann constant; T the absolute temperature; $\mathbf{Z}(t)$ a standard multi-dimensional Brownian motion and a Wiener process; $\mathbf{F}(\mathbf{R})$ is the internal force exerted by a polymer and depends on the given model. The stress is computed via the following classical Kramers' expression

$$\tau_p(\mathbf{x},t) = -n_p\langle\mathbf{R}\otimes\mathbf{F}(\mathbf{R})\rangle - n_p k_B T d\mathbf{I}, \tag{6}$$

where n_p is the density of dumbbells; $\mathbf{I}$ the identity tensor; d the spatial dimension of the problem; and $\otimes$ the tensorial product.

In (5), the term $\mathbf{u}(t,\mathbf{x})\cdot\nabla\mathbf{R}(t,\mathbf{x})$ accounts for the convection of the configuration fields by the flow. It can be seen that the existence of this convective term in this Eulerian framework is completely equivalent to the particle tracking in the traditional Lagrangian CONNFFESSIT approach [Hulsen, van Heel, and van den Brule (1997)].

For the Hookean and FENE models, the spring forces ($\mathbf{F}$) are respectively given by

$$\mathbf{F}_{Hookean} = H\mathbf{R}, \tag{7}$$

$$\mathbf{F}_{FENE} = \frac{H\mathbf{R}}{1-\|\mathbf{R}\|^2/(bk_BT/H)}, \tag{8}$$

where b is a non-dimensional parameter relating to the maximal polymer length and H is a spring constant.

4 A continuum-micro multiscale simulation approach

Gathering the partial differential equations (PDEs) (1) and (2), stochastic differential equations (SDEs) (5) and the Kramers' expression (6) yields a continuum-microscopic multi-scale system as follows [Ottinger (1996); Jourdain, Lelièvre, and

Bris (2002); Tran-Canh and Tran-Cong (2004)].

$$\rho\left(\frac{\partial \mathbf{u}}{\partial t}+\mathbf{u}\cdot\nabla\mathbf{u}\right)-\eta\Delta\mathbf{u}+\nabla p=\nabla\cdot\tau_p, \tag{9}$$

$$\nabla\cdot\mathbf{u}(t,x)=0, \tag{10}$$

$$d\mathbf{R}(t,\mathbf{x})+\mathbf{u}\cdot\nabla\mathbf{R}dt=\left[\nabla\mathbf{u}\mathbf{R}-\frac{2}{\zeta}\mathbf{F}(\mathbf{R})\right]dt+2\sqrt{\frac{kT}{\zeta}}d\mathbf{Z}(t), \tag{11}$$

$$\tau_p=n_p\left\{E\left[\mathbf{R}(t,\mathbf{x})\otimes\mathbf{F}(\mathbf{R}(t,\mathbf{x}))\right]-kTd\mathbf{I}\right\}. \tag{12}$$

The corresponding dimensionless forms of the system (9)-(12) and (7)-(8) are given by

$$Re\left(\frac{\partial \mathbf{u}}{\partial t}+\mathbf{u}\cdot\nabla\mathbf{u}\right)-(1-\varepsilon)\Delta\mathbf{u}+\nabla p=\nabla\cdot\tau_p, \tag{13}$$

$$\nabla\cdot\mathbf{u}(t,x)=0, \tag{14}$$

$$d\mathbf{R}(t,\mathbf{x})+\mathbf{u}\cdot\nabla\mathbf{R}dt=\nabla\mathbf{u}\mathbf{R}dt-\frac{1}{2We}\mathbf{F}(\mathbf{R})dt+\frac{1}{\sqrt{We}}d\mathbf{Z}(t), \tag{15}$$

$$\tau_p=\frac{\varepsilon}{We}\left\{E\left[\mathbf{R}(t,\mathbf{x})\otimes\mathbf{F}(\mathbf{R}(t,\mathbf{x}))\right]-d\mathbf{I}\right\}, \tag{16}$$

$$\mathbf{F}_{Hookean} = \mathbf{R}, \tag{17}$$

$$\mathbf{F}_{FENE} = \frac{\mathbf{R}}{1-\frac{\|\mathbf{R}\|^2}{b}}, \tag{18}$$

where $Re=\rho UL/\eta_o$ and $We=\lambda_H U/L$ are the Reynolds and Weissenberg numbers, respectively; $\varepsilon=\eta_p/\eta_o$ the ratio of polymer viscosity to the total one η_o ($\eta_o=\eta_s+\eta_p$), with $\eta_p=n_p k_B T\lambda_H$ being the polymer viscosity; $\lambda_H=\zeta/4H$ the relaxation time of the polymer chains; $L=\sqrt{kT/H}$ the characteristic length scale; U the characteristic velocity. Other parameters are defined as before.

Once $\mathbf{R}(t,\mathbf{x})$ is determined by solving (15), τ_p is computed by (16) and introduced into (13) and (14) as a known quantity for the solution of $\mathbf{u}$ and p. Thus the iterative process is initiated by an initial guess of the velocity and pressure fields.

5 Solving the continuum-micro multiscale system with an IRBF-control volume and the Brownian Configuration Field method

In this section, computational techniques are described for the numerical solution of the microscopic equation (i.e. SDE) and the conservation equations (i.e. PDEs), respectively. For the stochastic process, a variance reduction technique is also overviewed, followed by a presentation of the overall algorithm.

5.1 Numerical solution of the SDEs

In the present work, we use both Predictor-Corrector and explicit Euler schemes but only the latter is presented in detail. Let $\mathbf{R}_i = \mathbf{R}(t_i)$, using a fixed time step Δt for the stochastic process (15), the predicted BCF $\mathbf{R}_{i+1}$ at time t_{i+1} is explicitly determined as follows [Ottinger (1996); Kloeden and Platen (1997)].

$$\mathbf{R}_{i+1} = \mathbf{R}_i + \left[\nabla \mathbf{u}_i \cdot \mathbf{R}_i - \mathbf{u}_i \cdot \nabla \mathbf{R}_i - \frac{1}{2We}\mathbf{F}(\mathbf{R}_i)\right]\Delta t + \sqrt{\frac{\Delta t}{We}}\mathbf{Z}_i. \tag{19}$$

The updated configuration fields $\mathbf{R}_{i+1}$ are employed to estimate the polymer contribution to the predicted stress $(\tau_p)_{i+1}$, using the Kramers' expression (16), which is in turn used to determine the solution of the velocity field at time t_{i+1} by solving Eqs. (13) and (14). The velocity, velocity gradient and configuration gradient at time t_{i+1} are determined with data obtained at time t_i using a 1D-IRBFN control volume method which is presented in section 5.3.

5.2 Control variate method for the dumbbell models

Noise reduction is crucial in the stochastic simulation of systems (13)-(15). Different variance reduction techniques are detailed in [Gardiner (1994)]. In this work, the control variate method is employed for the dumbbell models. The method uses a control variate $< \mathbf{R_c} >$ which is correlated with the random variable $\mathbf{R}$ and can be calculated by a deterministic method, to produce a better estimator of $< \mathbf{R} >$. At a nodal point (centre of each of the m control volumes), n dumbbells are assigned and numbered from $i = 1...n$. Dumbbells having the same index in the whole analysis domain have the same random number. A detailed implementation of the control variate method for the numerical calculation of the polymer contribution to stress can be found in, for example, [Bonvin and Picasso (1999); Tran-Canh and Tran-Cong (2004)] and is not repeated here.

5.3 The Integral RBFs based control volume (IRBFCV) method for solving the PDEs

The incompressibility condition (14) is here enforced via the penalty method as follows [Laso, Picasso, and Ottinger (1997)].

$$p = -p_e \nabla \cdot \mathbf{u},$$

where p_e is a sufficiently large penalty parameter. Eq. (13) is then rewritten as

$$Re\frac{\partial \mathbf{u}}{\partial t} + Re\mathbf{u} \cdot \nabla \mathbf{u} - (1-\varepsilon)\Delta \mathbf{u} - p_e \nabla(\nabla \cdot \mathbf{u}) - \nabla \cdot \tau_p = 0, \tag{20}$$

In order to solve Eq. (20), the problem domain is discretized using a set of nodal points. Each node $\mathbf{x}_i$ is surrounded by a control volume denoted by V_i. Integrating Eqs. (17) over a control volume V_i, leads to the following equation

$$\int_{V_i} \left(Re\frac{\partial \mathbf{u}}{\partial t} + Re\mathbf{u}\cdot\nabla\mathbf{u} - (1-\varepsilon)\Delta\mathbf{u} - p_e\nabla(\nabla\cdot\mathbf{u}) - \nabla\cdot\tau_p \right) dV = 0. \tag{21}$$

Application of the Gauss divergence theorem to Eq. (21) yields

$$Re\frac{\partial}{\partial t}\int_{V_i}\mathbf{u}dV + Re\int_{V_i}\mathbf{u}\cdot\nabla\mathbf{u}dV - (1-\varepsilon)\int_{S_i}\nabla\mathbf{u}\cdot\widehat{\mathbf{n}}dS - p_e\int_{S_i}(\nabla\cdot\mathbf{u})\widehat{\mathbf{n}}dS - \int_{S_i}\tau_p\cdot\widehat{\mathbf{n}}dS = 0. \tag{22}$$

where S_i is the boundary of V_i; $\widehat{\mathbf{n}}$ a unit outward vector normal to S_i and dS a differential element of S_i. In order to approximate the solution of Eq. (22), a 1D-IRBF based control volume scheme is employed.

5.3.1 Review of 1D-IRBF method for spatial discretisation of differential equations

At a time t, the highest-order derivative of a dependent variable $u(x,t)$ (the second order in the case of this work) is decomposed as [Mai-Duy and Tran-Cong (2001)]

$$\frac{\partial^2 u(x,t)}{\partial x^2} = \sum_{i=1}^{m} w_i(t)G_i^{[2]}(x), \tag{23}$$

where m is the number of grid lines parallel to the y-direction; $\{w_i(t)\}_{i=1}^m$ the set of RBF weights; $\{G_i^{[2]}(x)\}_{i=1}^m$ the set of RBFs. Generally, the multi-quadric RBF (MQ-RBF) is considered as one of the best RBFs for the approximation of a function [Franke (1982)] and given by

$$G_i^{[2]}(x) = \left((x-c_i)^2 + a_i^2\right)^{1/2},$$

where $\{c_i\}_{i=1}^m$ is a set of centres and $\{a_i\}_{i=1}^m$ a set of MQ-RBF widths. A set of collocation points $\{x_i\}_{i=1}^m$ is taken to be the set of centres, while the RBF width is chosen as follows

$$a_i = \beta d_i,$$

where β is a factor and d_i is the distance from the i^{th} centre to its nearest neighbour. The corresponding first-order derivative and function itself are then determined through integration as follows.

$$\frac{\partial u(x,t)}{\partial x} = \sum_{i=1}^{m} w_i(t)G_i^{[1]}(x) + C_1(t), \tag{24}$$

$$u(x,t) = \sum_{i=1}^{m} w_i(t) G_i^{[0]}(x) + C_1(t)x + C_2(t), \tag{25}$$

where $G_i^{[1]}(x) = \int G_i^{[2]}(x)dx$, $G_i^{[0]}(x) = \int G_i^{[1]}(x)dx$ and C_1 and C_2 are unknown constants of integration at time t.

Collocating equations (23), (24) and (25) at grid points $\{x_i\}_{i=1}^{m}$ yields the following set of algebraic equations

$$\frac{\partial^2 \widetilde{\mathbf{u}}(x,t)}{\partial x^2} = \widetilde{\mathbf{G}}^{[2]}(x)\widetilde{\mathbf{w}}(t), \tag{26}$$

$$\frac{\partial \widetilde{\mathbf{u}}(x,t)}{\partial x} = \widetilde{\mathbf{G}}^{[1]}(x)\widetilde{\mathbf{w}}(t), \tag{27}$$

$$\widetilde{\mathbf{u}}(x,t) = \widetilde{\mathbf{G}}^{[0]}(x)\widetilde{\mathbf{w}}(t), \tag{28}$$

where

$$\widetilde{\mathbf{G}}^{[2]} = \begin{bmatrix} G_1^{[2]}(x_1) & G_2^{[2]}(x_1) & \cdots & G_m^{[2]}(x_1) & 0 & 0 \\ G_1^{[2]}(x_2) & G_2^{[2]}(x_2) & \cdots & G_m^{[2]}(x_2) & 0 & 0 \\ \vdots & \vdots & \ddots & \vdots & \vdots & \vdots \\ G_1^{[2]}(x_m) & G_2^{[2]}(x_m) & \cdots & G_m^{[2]}(x_m) & 0 & 0 \end{bmatrix},$$

$$\widetilde{\mathbf{G}}^{[1]} = \begin{bmatrix} G_1^{[1]}(x_1) & G_2^{[1]}(x_1) & \cdots & G_m^{[1]}(x_1) & 1 & 0 \\ G_1^{[1]}(x_2) & G_2^{[1]}(x_2) & \cdots & G_m^{[1]}(x_2) & 1 & 0 \\ \vdots & \vdots & \ddots & \vdots & \vdots & \vdots \\ G_1^{[1]}(x_m) & G_2^{[1]}(x_m) & \cdots & G_m^{[1]}(x_m) & 1 & 0 \end{bmatrix},$$

$$\widetilde{\mathbf{G}}^{[0]} = \begin{bmatrix} G_1^{[0]}(x_1) & G_2^{[0]}(x_1) & \cdots & G_m^{[0]}(x_1) & x_1 & 1 \\ G_1^{[0]}(x_2) & G_2^{[0]}(x_2) & \cdots & G_m^{[0]}(x_2) & x_2 & 1 \\ \vdots & \vdots & \ddots & \vdots & \vdots & \vdots \\ G_1^{[0]}(x_m) & G_2^{[0]}(x_m) & \cdots & G_m^{[0]}(x_m) & x_m & 1 \end{bmatrix},$$

$$\begin{aligned} \widetilde{\mathbf{w}}(t) &= (w_1(t), w_2(t), \cdots, w_m(t), C_1(t), C_2(t))^T, \\ \widetilde{\mathbf{u}}(x,t) &= (u_1(x,t), u_2(x,t), \cdots, u_m(x,t))^T, \\ \frac{d^k \widetilde{\mathbf{u}}(x,t)}{dx^k} &= \left(\frac{d^k u_1(x,t)}{dx^k}, \frac{d^k u_2(x,t)}{dx^k}, \cdots, \frac{d^k u_{N_x}(x,t)}{dx^k} \right)^T, \end{aligned}$$

where $u_i = u(x_i,t)$ with $i = \{1,2,\cdots,m\}$.

The use of integration to construct the RBF approximants is expected to avoid the deterioration of accuracy caused by differentiation [Mai-Duy and Tran-Cong (2001)].

5.3.2 The integrated RBFs based control volume (IRBFCV) method

The 1D-IRBFs scheme described in section 5.3.1 is introduced into the control volume formulation Eq. (22) to approximate the field variables as well as their derivatives. In this work, the problem domain is discretised using a Cartesian grid. On a grid line, 1D-IRBFs are employed to represent the unknown field variables and their derivatives. Control volumes are generated around collocation points $(\{x_i\}_{i=1}^{m})$ (see Fig.1). In this conservative scheme, the governing equations are forced to be satisfied locally over control volumes and the boundary conditions are directly imposed on the relevant IRBF approximants. The procedure leads to an algebraic equation system for unknown nodal values of the field variable. Owing to the presence of integration constants in the IRBF based approximants, one can introduce in the algebraic equation system additional information such as nodal derivative values (more details can be found in [Mai-Duy and Tran-Cong (2010)]. Thus, the algebraic equation system (28) can be reformulated as

$$\begin{pmatrix} \widetilde{\mathbf{u}} \\ \mathbf{f} \end{pmatrix} = \begin{bmatrix} \widetilde{\mathbf{G}}^{[0]} \\ \mathbf{L} \end{bmatrix} \widetilde{\mathbf{w}}(t) = \mathbf{C}\widetilde{\mathbf{w}}(t). \tag{29}$$

The conversion of the network-weight space into the physical space is achieved by inverting (29)

$$\widetilde{\mathbf{w}}(t) = \mathbf{C}^{-1} \begin{pmatrix} \widetilde{\mathbf{u}} \\ \mathbf{f} \end{pmatrix}, \tag{30}$$

where $\mathbf{f} = \mathbf{L}\widetilde{\mathbf{w}}$ represents additional information; $\mathbf{C}^{-1}$ is the conversion matrix; $\widetilde{\mathbf{G}}^{[0]}$ and $\widetilde{\mathbf{w}}$ are defined as before. By substituting (30) into (26) and (27), the second and first-order derivatives of $u(x,t)$ will be expressed in terms of nodal variable values as follows.

$$\begin{aligned} \tfrac{\partial^2 u(x,t)}{\partial^2 x} &= \mathscr{D}_{2x}\widetilde{\mathbf{u}}(x,t) + k_{2x}, \\ \tfrac{\partial u(x,t)}{\partial x} &= \mathscr{D}_{1x}\widetilde{\mathbf{u}}(x,t) + k_{1x}, \end{aligned} \tag{31}$$

where $\mathscr{D}_{1x}$ and $\mathscr{D}_{2x}$ are known vectors of length m; and k_{2x} and k_{1x} scalars. Applying (31) at each and every collocation point on the gridline yields

$$\begin{aligned} \tfrac{\partial^2 \widetilde{\mathbf{u}}(x,t)}{\partial^2 x} &= \widetilde{\mathscr{D}}_{2x}\widetilde{\mathbf{u}}(x,t) + \widetilde{k}_{2x}, \\ \tfrac{\partial \widetilde{\mathbf{u}}(x,t)}{\partial x} &= \widetilde{\mathscr{D}}_{1x}\widetilde{\mathbf{u}}(x,t) + \widetilde{k}_{1x}, \end{aligned} \tag{32}$$

where $\widetilde{\mathscr{D}}_{2x}$ and $\widetilde{\mathscr{D}}_{1x}$ are known matrices of dimension $m \times m$; and $\widetilde{k}_{2x}$ and $\widetilde{k}_{1x}$ are known vectors of length m. Further details are revealed as numerical examples are described below.

5.4 Algorithm of the present procedure

The present multi-scale continuum-microscopic method can now be described in an overall detailed algorithm as follows.

a. Generate a set of Cartesian grid collocation points and the associated CVs. Start with an initial guess of the velocity field and molecular configurations for the first iteration together with the given initial and boundary conditions of the problem. In the present work, the initial velocity field is set to zero. Assign n dumbbells to each collocation point. Initial n molecular configurations are sampled from equilibrium Gaussian distribution [Ottinger (1996)]. The control variates $\widehat{\mathbf{R}}_i$ associated with the configuration fields $\mathbf{R}_i$ are created. All dumbbells having the same index constitute a configuration. Hence, there is an ensemble of n configuration fields $\mathbf{R}_i$ $(i = 1...n)$. Since all the dumbbells having the same index receive the same random numbers, there is a strong correlation between dumbbells in a configuration. Compute τ_p at nodal points;

b. Calculate unknown velocity and pressure fields using the IRBFCV method described in section 5.3;

c. Calculate the polymer configuration fields by the method described in section 5.1. For each configuration field $\mathbf{R}_i$, a corresponding control variate is determined;

d. Determine the polymer contribution to stress τ_p at nodal points (the centres of CVs) by taking the ensemble average of the polymer configurations in each CV, using Eq. (16);

e. Calculate a convergence measure (CM) based on the velocity field, which is defined by

$$CM = \sqrt{\frac{\sum_{j=1}^{m}\sum_{i=1}^{d}\left(u_{i,j}^{t}-u_{i,j}^{t-1}\right)^2}{\sum_{j=1}^{m}\sum_{i=1}^{d}\left(u_{i,j}^{t}\right)^2}} \leq tol, \tag{33}$$

where d is the number of dimensions; tol a preset tolerance; $u_{i,j}$ the i component of the velocity at a collocation point j; m the total number of collocation points and t is the iteration number;

f. If steady state or a given time is reached, terminate the simulation. Otherwise return to step b for the next time level of the simulation process.

6 Numerical examples

The present method is verified with the simulation of the start-up planar Couette flows of the Hookean and FENE model fluids. This problem, defined in Figure 1, was earlier studied with different methods by [Mochimaru (1983); Laso and Ottinger (1993); Tran-Canh and Tran-Cong (2002, 2004); Tran, An-Vo, Mai-Duy, and Tran-Cong (2011)]. For time $t < 0$, the fluid is at rest. At $t = 0$, the lower plate starts to move with a constant velocity $V = 1$. No-slip condition is assumed at the wall. For the start-up Couette flows, the governing equations (13)-(16), are reduced as follows. Let $\tau_{p,yx} = \tau_{yx}$ in this case.

$$Re\frac{\partial u}{\partial t}(t,y) - (1-\varepsilon)\frac{\partial^2 u}{\partial y^2}(t,y) = \frac{\partial \tau_{yx}}{\partial y}(t,y), \tag{34}$$

$$dP(t,y) = \left(-\frac{1}{2We}F_P(\mathbf{R}(t,y)) + \frac{\partial u}{\partial y}(t,y)\,Q(t,y)\right)dt + \frac{1}{\sqrt{We}}dV(t), \tag{35}$$

$$dQ(t,y) = -\frac{1}{2We}F_Q(\mathbf{R}(t,y))\,dt + \frac{1}{\sqrt{We}}dW(t), \tag{36}$$

$$\tau_{yx}(t,y) = -\frac{\varepsilon}{We}E(P(t,y)\,Q(t,y)), \tag{37}$$

where u is the x-velocity; τ_{yx} the shear stress; (P,Q) the components of a BCF process $\mathbf{R}(t,y)$; (V,W) two dimensional Brownian motions of a dumbbell's configuration; and (F_P,F_Q) two components of the force $\mathbf{F}(\mathbf{R})$. Here we will describe the time and space discretisation of the problem involving Hookean dumbbell model only and similar description for the FENE dumbbell model is straightforward.

6.1 The Hookean dumbbell model

For the Hookean model, Eqs. (35)-(36) are rewritten as follows.

$$dP(t,y) = \left(-\frac{1}{2We}P(t,y) + \frac{\partial u}{\partial y}(t,y)\,Q(t,y)\right)dt + \frac{1}{\sqrt{We}}dV(t), \tag{38}$$

$$dQ(t,y) = -\frac{1}{2We}Q(t,y)\,dt + \frac{1}{\sqrt{We}}dW(t). \tag{39}$$

The chosen parameters are Weissenberg number $We = 0.5$; Reynolds number $Re = 0.1$ and ratio $\varepsilon = 0.9$. The equations (34), (38), (39) and (37) are solved through two steps as described below.

6.1.1 Discretisation of the micro-scale stochastic governing equation

Given that the velocity field is previously determined at time t_i, Eqs (38)-(39) are discretized using the Euler explicit scheme with n $(n = 1000)$ realizations for each

random process as follows.

$$P^k_{i+1,j} = \left(1-\frac{\delta t}{2}\right) P^k_{i,j} + \underbrace{\left(\frac{\partial u_j}{\partial y}\right)^k_{i+1} \Delta t}_{\mathscr{M}^k_{i+1,j}} Q^k_i + \delta V^k_{i,j}\sqrt{\delta t}, \tag{40}$$

$$Q^k_{i+1} = \left(1-\frac{\delta t}{2}\right) Q^k_i + \delta W^k_i \sqrt{\delta t}, \tag{41}$$

where $\delta t = \frac{\Delta t}{We}$; i and j stand for the time and space discretizations respectively; k ($1 \le k \le n$) stands for the realisation of random processes; and $\delta V^k_{i,j}$ and δW^k_i are standard norm based random variables.

It is noted that (i) $\mathscr{M}^k_{i+1,j}$ are the parameters obtained by the discretisation of macroscopic governing equation Eq. (34) at time t_{i+1} and collocation points y_j (see section 6.1.2); and (ii) Q^k_i are independent of their position y owing to the geometrical characteristic of the problem.

The shear stress τ_{yx} is then calculated using the coupling equation Eq. (37) as

$$(\tau_{yx})_{i+1,j} = \frac{\varepsilon}{We}\frac{1}{n}\sum_{k=1}^{n} P^k_{i+1,j} Q^k_{i+1}. \tag{42}$$

The shear stresses $(\tau_{yx})_{i+1,j}$ at time t_{i+1} and collocation points y_j ($1 \le j \le m$) are employed to solve the momentum governing equation (34) as described next.

6.1.2 Discretization of the macro-scale governing equation

Considering Eq. (34) with the following initial and boundary conditions

- Initial conditions

  $u(0,0) = V = 1 \quad \text{and} \quad u(0,y) = 0 \quad \forall y \neq 0.$

- Dirichlet boundary conditions

  $u(t,0) = V = 1 \;\; \forall t > 0; \quad u(t,L) = 0 \quad \forall t > 0.$

The spatial domain ($0 \le y \le 1$) is discretised with m nodal points and time domain ($0 \le t \le t_f$, t_f is a time when the flow has reached its steady state) with a constant time step Δt.

Each collocation point y_j is surrounded by a control volume Ω_j defined as $[y_{j-1/2}$, $y_{j+1/2}]$ (see Fig. 1). For the end nodal points ($j = 1$ and $j = m$), the control

volumes are $\Omega_1 = [y_1, y_{1+1/2}]$ and $\Omega_m = [y_{m-1/2}, y_m]$ respectively. Integration of Eq. (34) over Ω_j yields

$$Re\frac{\partial}{\partial t}\int_{y_{j-1/2}}^{y_{j+1/2}} u(t,y)\,dy - (1-\varepsilon)\int_{y_{j-1/2}}^{y_{j+1/2}} \frac{\partial^2 u}{\partial y^2}(t,y)\,dy = \int_{y_{j-1/2}}^{y_{j+1/2}} \frac{\partial \tau_{yx}}{\partial y}(t,y)\,dy. \quad (43)$$

Assuming that u is linear over the time interval $\Delta t = [t_i,\ t_{i+1}]$, Eq. (43) can be written as follows.

$$\frac{Re}{\Delta t}\int_{y_{j-1/2}}^{y_{j+1/2}} u(t_{i+1},y)\,dy - \frac{Re}{\Delta t}\int_{y_{j-1/2}}^{y_{j+1/2}} u(t_i,y)\,dy - (1-\varepsilon)\frac{\partial u}{\partial y}\left(t_{i+1}, y_{j+1/2}\right) + (1-\varepsilon)\frac{\partial u}{\partial y}\left(t_{i+1}, y_{j-1/2}\right) = \tau_{yx}\left(t_i, y_{j+1/2}\right) - \tau_{yx}\left(t_i, y_{j-1/2}\right), \quad (44)$$

or

$$-\alpha\frac{du_{i+1}}{dy}\left(y_{j+1/2}\right) + \alpha\frac{du_{i+1}}{dy}\left(y_{j-1/2}\right) + \gamma\int_{y_{j-1/2}}^{y_{j+1/2}} u_{i+1}(y)\,dy = \tau_{yx,i}\left(y_{j+1/2}\right) - \tau_{yx,i}\left(y_{j-1/2}\right) + \gamma\int_{y_{j-1/2}}^{y_{j+1/2}} u_i(y)\,dy, \quad (45)$$

where $\gamma = Re/\triangle t$; $\alpha = 1-\varepsilon$; $u_i(y) = u(t_i,y)$ and $\tau_{yx,i}(y) = \tau_{yx}(t_i,y)$ with $u_0(y) = u(0,y)$ and $\tau_{yx,0}(y) = \tau_{yx}(0,y)$.

Making use of (23)-(25) and (29)-(30), the values of u_{i+1}, du_{i+1}/dy and d^2u_{i+1}/dy^2 in (45) at time t_{i+1} and an arbitrary point y in the domain under consideration can be determined in terms of the nodal values $u_{i+1,j}$ as follows.

$$\begin{aligned} u_{i+1}(y) &= \left[\mathbf{G}_1^{[0]}(y), \mathbf{G}_2^{[0]}(y), \cdots, \mathbf{G}_m^{[0]}(y), y, 1\right]\mathbf{C}^{-1}\widetilde{\mathbf{u}}_{i+1,j} \\ &= \sum_{j=1}^{m}\varphi_j(y)\,u_{i+1,j}, \quad (46) \\ \frac{du_{i+1}}{dy}(y) &= \left[\mathbf{G}_1^{[1]}(y), \mathbf{G}_2^{[1]}(y), \cdots, \mathbf{G}_m^{[1]}(y), 1, 0\right]\mathbf{C}^{-1}\widetilde{\mathbf{u}}_{i+1,j} \\ &= \sum_{j=1}^{m}\frac{d\varphi_j}{dy}(y)\,u_{i+1,j}, \quad (47) \\ \frac{d^2u_{i+1}}{dy^2}(y) &= \left[\mathbf{G}_1^{[2]}(y), \mathbf{G}_2^{[2]}(y), \cdots, \mathbf{G}_m^{[2]}(y), 0, 0\right]\mathbf{C}^{-1}\widetilde{\mathbf{u}}_{i+1,j} \\ &= \sum_{j=1}^{m}\frac{d^2\varphi_j}{dy^2}(y)\,u_{i+1,j}, \quad (48) \end{aligned}$$

where φ_j's are new basis functions in the physical space.

The integrals in (45) are calculated using Gauss quadrature. Making use of Eqs. (46)-(48), the evaluation of Eq. (45) with $j \in [2,3,\cdots,m-1]$ generates a system of algebraic equations in terms of the unknown nodal values of u_{i+1} at the internal collocation points and time t_{i+1}.

In this work, we use a time step $\triangle t = 2 \times 10^{-2}$, ($\Delta t = 10^{-4}$ in [Laso and Ottinger (1993); Mochimaru (1983)] and $\Delta t = 10^{-2}$ in [Tran-Canh and Tran-Cong (2002, 2004); Tran, An-Vo, Mai-Duy, and Tran-Cong (2011)]) and a relatively coarse spatial discretization $\Delta y = 0.05$ (i.e. the number of collocation points is $m = 21$). The approximated results are in good agreement with ones obtained using the other methods mentioned above. Indeed, Figure 2 shows the evolution of the velocity at four locations $y = 0.2,\ 0.4,\ 0.6$ and 0.8 in comparison with ones using the IRBF-BCF collocation method [Tran, An-Vo, Mai-Duy, and Tran-Cong (2011)], with $\Delta t = 0.01$ and $\Delta y = 0.05$. Figure 3 depicts the evolution of the shear stress at four locations $y = 0.2,\ 0.4,\ 0.6$ and 0.8 in comparison with the results by the IRBF-BCF collocation method. Figure 4, describing the evolution of the stress profile at the location $y = 0.2$, shows that the present method significantly reduces noises in the approximation of a random process. This is reinforced by the good convergence measure (CM) obtained for a stochastic approach as shown in Figure 5. Furthermore, the results by the present method are also in very good agreement with ones obtained from a macroscopic approach (the Finite Difference Method (FDM)) for the Oldroyd-B model fluid (corresponding to the Hookean dumbbell model fluid) with $\Delta t = 0.01$ and $\Delta y = 0.01$ at the steady state for both velocity and stress fields. However, there is a small difference at the unsteady state (Figure 6).

Finally, using coarser numbers of collocation points ($m = 11$, $m = 15$ and $m = 17$), the results showed that the present method is able to produce a high degree of accuracy with a relatively coarse grid. For example, Figure 7 depicts the evolution of the shear stress (left figure) and the velocity at the location $y = 0.2$ using 11 grid points.

6.2 The FENE dumbbell model

For the FENE dumbbell model, equations (35)-(37) are rewritten as

$$dP(t,y) = \left(-\frac{1}{2We}\frac{P(t,y)}{1-\frac{\|R\|^2}{b}} + \frac{\partial u}{\partial y}(t,y)\,Q(t,y) \right) dt + \frac{1}{\sqrt{We}} dV(t), \tag{49}$$

$$dQ(t,y) = -\frac{1}{2We}\frac{Q(t,y)}{1-\frac{\|R\|^2}{b}} dt + \frac{1}{\sqrt{We}} dW(t), \tag{50}$$

$$\tau_{yx}(t,y) = -\frac{\varepsilon}{We}\frac{1}{n}\left(\frac{P(t,y)\,Q(t,y)}{1-\frac{\|R\|^2}{b}} \right), \tag{51}$$

where $\|R\|^2 = P^2 + Q^2$. The problem is solved with the following chosen physical parameters: $\eta_o = \eta_s + \eta_p = 1$; $\rho = 1.2757$; $\lambda_H = 49.62$; $\eta_s = 0.0521$ and $b = 50$ as in [Laso and Ottinger (1993); Tran-Canh and Tran-Cong (2004); Tran, An-Vo, Mai-Duy, and Tran-Cong (2011)], where η_s, η_p, ρ, λ_H are defined as before. The corresponding Weissenberg, Reynolds numbers and the ratio ε are given by

$$Re = \frac{\rho VL}{\eta_0} = 1.2757; \quad We = \frac{\lambda_H V}{L} = 49.62; \quad \varepsilon = \frac{\eta_p}{\eta_o} = 0.9479; \tag{52}$$

For this case, the Predictor-Corrector method is employed to discretize the SDEs (49)-(50). Figure 8 shows evolutions of the velocity (left figure) and shear stress (right figure) of the FENE dumbell model fluid at four locations $y = 0.2$, $y = 0.4$, $y = 0.6$ and $y = 0.8$, using 11 collocation points, time step $\triangle t = 0.02$ and 2000 dumbbells assigned in each control volume. Although with a coarser grid of collocation points (i.e. the number of grid points is 11), the approximated results of the present method are in very good agreement with those of various approaches [Laso and Ottinger (1993); Tran-Canh and Tran-Cong (2002, 2004)].

7 Concluding remarks

This paper reports the development of a continuum-micro multi-scale method for the simulation of flow of dilute polymer solutions using a combination of the Integrated Radial Basis Function Control Volume method and the Brownian Configuration Field scheme. The method is verified with standard test problems. Advantages of the new approach include (i) to obviate the need for a closed form constitutive equation; (ii) to achieve very efficient Cartesian grid discretisation for the macro-scale equations; (iii) to improve the approximation accuracy; (iv) to avoid the reduction in convergence rate caused by differentiation; and (v) to reduce the white noise in the approximation via the use of integration as a smoothing operator.

Acknowledgement: This work was supported by the Australian Research Council.

References

Bird, R. B.; Armstrong, R. C.; Hassager, O. (1987): *Dynamics of polymeric liquids, V.2*. John Wiley & Sons:New York.

Bonvin, J.; Picasso, M. (1999): Variance reduction methods for connffessit–like simulations. *Journal of Non-Newtonian Fluid Mechanics*, vol. 84, pp. 191–215.

Chu, J.; Efendiev, W.; Ginting, V.; Hou, T. Y. (2008): Flow based over-sampling technique for multiscale finite element methods. *Advances in Water Resources*, vol. 31, pp. 599–608.

Engquist, B.; Lötstedt, P.; Runborg, O. (2000): *Multiscale Methods in Science and Engineering: Lecture Notes in Computational Science and Engineering V. 44*. Springer:Berlin.

Franke, R. (1982): Scattered data interpolation: tests of some methods. *Mathematics of Computation*, vol. 38, pp. 181–200.

Gardiner, C. W. (1994): *Handbook of Stochastic Methods for Physics, chemistry and the natural Sciences*. Springer:Berlin.

Hajibeygi, H.; Gonfigli, G.; Hesse, M. A.; Jenny, P. (2008): Iterative multiscale finite-volume method. *Journal of Computational Physics*, vol. 227, pp. 8604–8621.

Hou, T. Y. (2005): Multiscale modelling and computation of fluid flow. *International Journal for Numerical Methods in Fluids*, vol. 47, pp. 707–719.

Hulsen, M. A.; van Heel, A. P. G.; van den Brule, B. H. A. A. (1997): Simulation of viscoelastic flow using brownian configuration fields. *Journal of Non-Newtonian Fluid Mechanics*, vol. 70, pp. 79–101.

Jourdain, B.; Lelièvre, T.; Bris, C. L. (2002): Numerical analysis of micro-macro simulations of polymeric fluid flows: a simple case. *Mathematical Models and Methods in Applied Sciences*, vol. 12, pp. 1205–1243.

Keunings, R. (2004): Micro-macro methods for the multiscale simulation of viscoelastic flows using molecular models of kinetic theory, rheology review 2004. *D.M. Binding and K. Walters, Eds., British Society of Rheology*, pp. 67–98.

Kevorkian, J.; Cole, J. D. (1996): *Multiple scale and singular perturbation method*. Springer: New-York.

Kloeden, P. E.; Platen, E. (1997): *Numerical solution of stochastic differential equations*. Springer:Berlin.

Laso, M.; Ottinger, H. C. (1993): Calculation of viscoelastic flow using molecular models: the connffessit approach. *Journal of Non-Newtonian Fluid Mechanics*, vol. 47, pp. 1–20.

Laso, M.; Picasso, M.; Ottinger, H. C. (1997): 2-d time-dependent viscoelastic flow calculation using connffessit. *AIChE Journal*, vol. 43, pp. 877–892.

Mai-Duy, N.; Tran-Cong, T. (2001): Numerical solution of Navier-Stokes equations using multiquadric radial basis function networks. *International Journal for Numerical Method in Fluids*, vol. vol. 37, pp. 65–86.

Mai-Duy, N.; Tran-Cong, T. (2010): A control volume technique based on integrated RBFNs for the convection-diffusion equation. *Numerical Methods for Partial Differential Equations*, vol. 26, pp. 426–447.

Maslov, V. P.; Fedoriuk, M. V. (1981): *Semiclassical approximation in Quantum mechanics*. D. Reidel, Dordrecht: Boston.

Mochimaru, Y. (1983): Unsteady-state development of plane couette flow for viscoelastic fluids. *Journal of Non-Newtonian Fluid Mechanics*, vol. 12, pp. 135–152.

Ottinger, H. (1996): *Stochastic processes in Polymeric Fluids*. Springer:Berlin.

Somasi, M.; Khomami, B. (2001): A new approach for studying the hydrodynamic stability of fluids with microstructure. *Phys. Fluids*, vol. 13, pp. 1811–1814.

Tran, C. D.; An-Vo, D. A.; Mai-Duy, N.; Tran-Cong, T. (2011): An integrated rbfn-based macro-micro multi-scale method for computation of visco-elastic fluid flows. *CMES: Computer Modeling in Engineering & Sciences*, vol. 82, pp. 137–162.

Tran, C. D.; Phillips, D. G.; Tran-Cong, T. (2009): Computation of dilute polymer solution flows using bcf-rbfn based method and domain decomposition technique. *Korea Autralia Rheology Journal*, vol. 21, pp. 1–12.

Tran-Canh, D.; Tran-Cong, T. (2002): Computation of viscoelastic flow using neural networks and stochastic simulation. *Korea Autralia Rheology Journal*, vol. 14, pp. 161–174.

Tran-Canh, D.; Tran-Cong, T. (2004): Meshless simulation of dilute polymeric flows using brownian configuration fields. *Korea Autralia Rheology Journal*, vol. 16, pp. 1–15.

Weinan, E.; Engquist, B. (2003): Multiscale modeling and computation. *Notices of the AMS*, vol. 50, pp. 1062–1070.

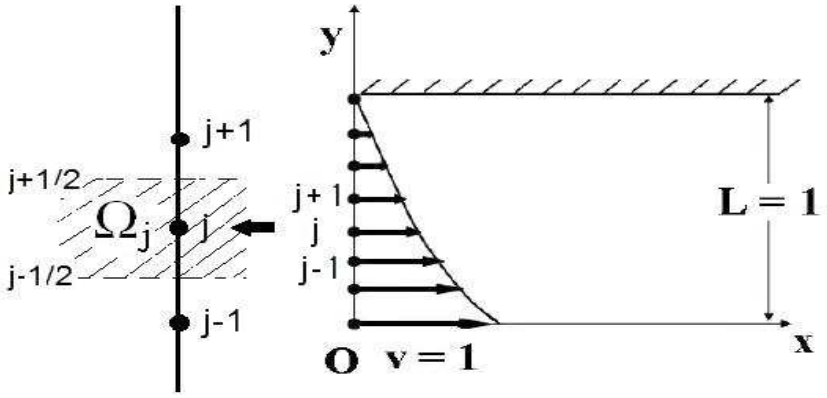

Figure 1: The start-up planar Couette flow problem: the bottom plate moves with a constant velocity $V = 1$, the top plate is fixed; no-slip boundary condition is applied at the fluid solid interfaces. The collocation point distribution is only schematic.

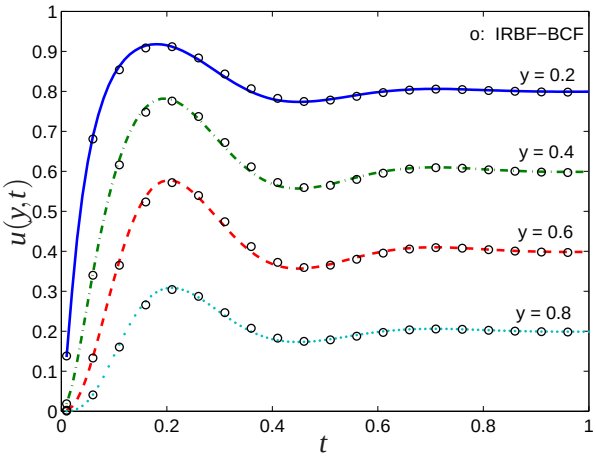

Figure 2: The start up planar Couette flow (Fig. 1) of the Hookean dumbbell model fluid: the parameters of the problem are number of dumbbells $n = 1000$, number of collocation points $m = 21$, $\Delta t = 0.02$, Weissenberg Number $We = 0.5$; Reynolds Number $Re = 0.1$ and the ratio $\varepsilon = 0.9$. The evolution of the velocity at locations $y = 0.2$, $y = 0.4$, $y = 0.6$ and $y = 0.8$ using the present method (IRBFCV-BCF) and the IRBF-BCF method (Tran, An-Vo, Mai-Duy, and Tran-Cong (2011)).

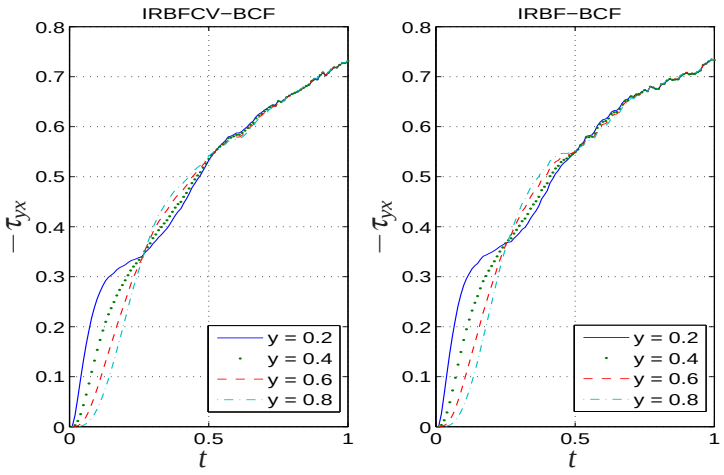

Figure 3: Start-up planar Couette flow of a Hookean dumbbell model fluid: The evolution of shear stress at the locations $y = 0.2$, $y = 0.4$, $y = 0.6$ and $y = 0.8$ using the present method (left figure) and the IRBF-BCF method (right figure) [Tran, An-Vo, Mai-Duy, and Tran-Cong (2011)].

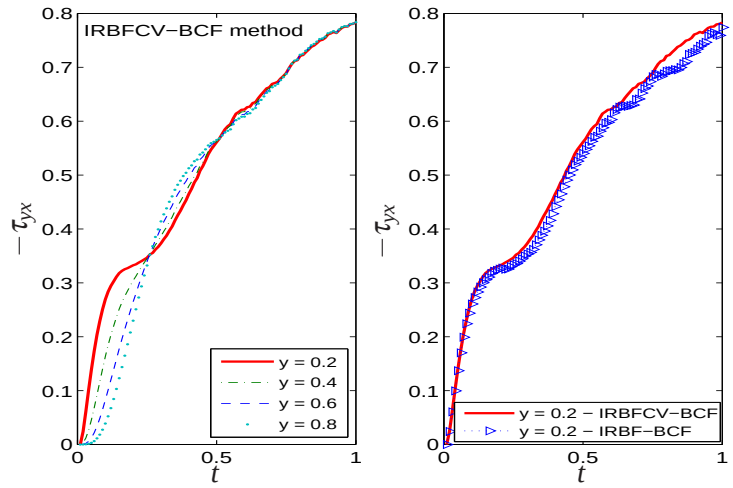

Figure 4: Start-up planar Couette flow of a Hookean dumbbell model fluid: The evolution of shear stress at the locations $y = 0.2$, $y = 0.4$, $y = 0.6$ and $y = 0.8$ using the present method (left figure); a comparison of the shear stress obtained at the location $y = 0.2$ by the present method and the IRBF-BCF method (right figure), [Tran, An-Vo, Mai-Duy, and Tran-Cong (2011)].

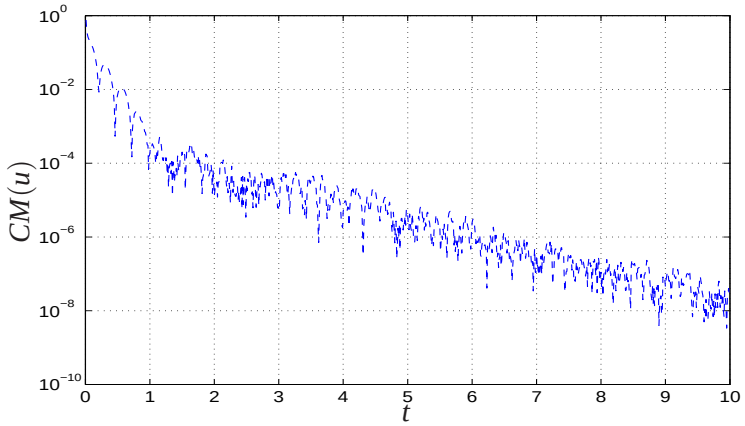

Figure 5: Start-up planar Couette flow of a Hookean dumbbell model fluid: the parameters of the problem are given in Figure 1 and the caption of Figure 2. The convergence measure (CM) for the velocity field is defined by (33).

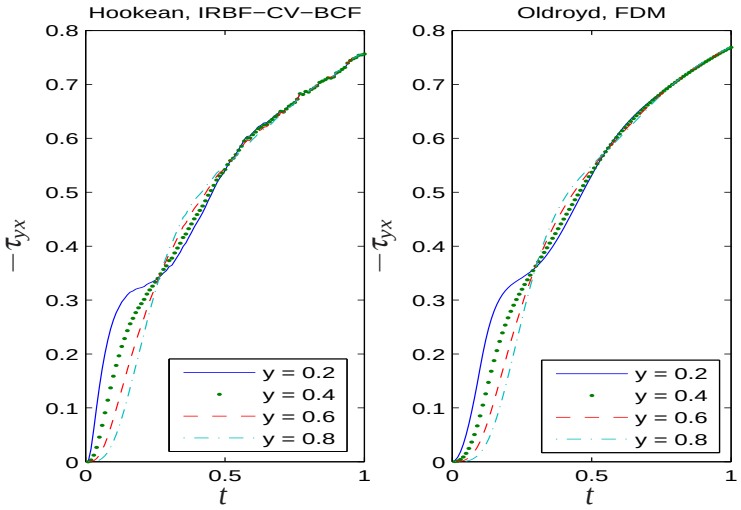

Figure 6: Start-up planar Couette flow of a Hookean dumbbell model fluid: The evolution of shear stress at the locations $y = 0.2$, $y = 0.4$, $y = 0.6$ and $y = 0.8$ using the present method (left figure) and the FDM for the oldroyd-B model fluid (right figure).

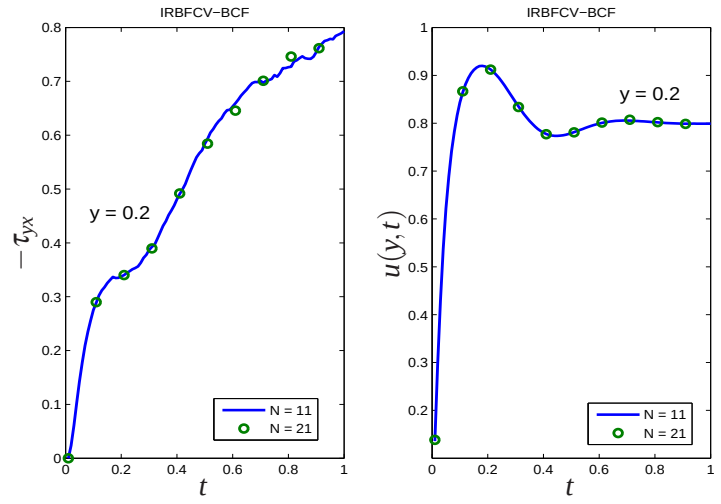

Figure 7: Start-up planar Couette flow of a Hookean dumbbell model fluid: The evolution of velocity (right figure) and shear stress (left figure) at the location $y = 0.2$ using 21 and 11 collocation points.

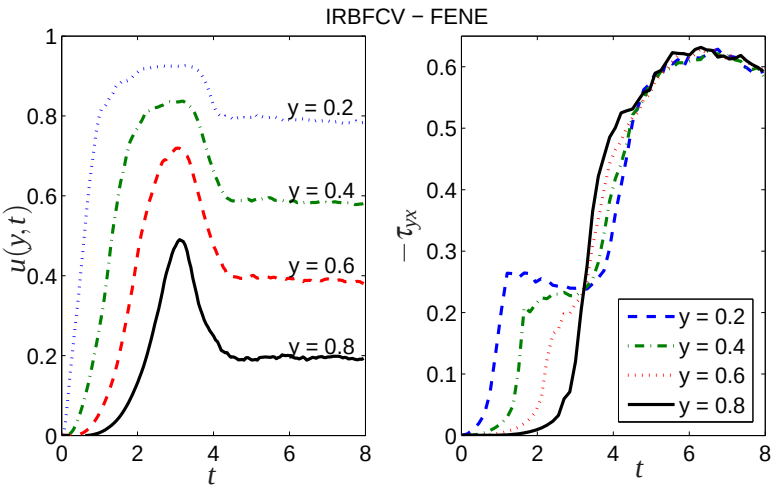

Figure 8: The start-up planar Couette flow of the FENE dumbbell model fluid: The parameters of the problem are shown in Fig. 1. The evolutions of the velocity (left figure) and the shear stress (right figure) at locations y = 0.2, y = 0.4, y = 0.6 and y = 0.8.